

FGAA-FPN: Foreground-Guided Angle-Aware Feature Pyramid Network for Oriented Object Detection

Jialin Ma^{1*}

¹International school of BUPT, Beijing University Of Posts And Telecommunications, Beijing, China.

Corresponding author(s). E-mail(s): majialin2023213633@bupt.edu.cn;

Abstract

With the increasing availability of high-resolution remote sensing and aerial imagery, oriented object detection has become a key capability for geographic information updating, maritime surveillance, and disaster response. However, it remains challenging due to cluttered backgrounds, severe scale variation, and large orientation changes. Existing approaches largely improve performance through multi-scale feature fusion with feature pyramid networks or contextual modeling with attention, but they often lack explicit foreground modeling and do not leverage geometric orientation priors, which limits feature discriminability. To overcome these limitations, we propose FGAA-FPN, a Foreground-Guided Angle-Aware Feature Pyramid Network for oriented object detection. FGAA-FPN is built on a hierarchical functional decomposition that accounts for the distinct spatial resolution and semantic abstraction across pyramid levels, thereby strengthening multi-scale representations. Concretely, a Foreground-Guided Feature Modulation module learns foreground saliency under weak supervision to enhance object regions and suppress background interference in low-level features. In parallel, an Angle-Aware Multi-Head Attention module encodes relative orientation relationships to guide global interactions among high-level semantic features. Extensive experiments on DOTA v1.0 and DOTA v1.5 demonstrate that FGAA-FPN achieves state-of-the-art results, reaching 75.5% and 68.3% mAP, respectively.

Keywords: Feature Pyramid Network, Foreground-Guided Feature Modulation, Angle-Aware Attention, oriented object detection

1 Introduction

Oriented object detection in high-resolution remote sensing imagery is a core capability for geographic information updating, maritime surveillance, and disaster monitoring. Compared with horizontal detection, remote sensing objects often appear with arbitrary orientations, large scale variation, and dense spatial layouts under cluttered backgrounds, which aggravates foreground–background entanglement and makes accurate localization more difficult [1, 2]. Improving oriented detection thus requires two complementary ingredients: discriminative multi-scale representations that remain robust to background interference, and explicit modeling of object geometry and orientation for reliable regression and classification.

Most mainstream remote sensing oriented detectors follow a two-stage paradigm, exemplified by Oriented R-CNN [3]. To cope with large scale variation and dense distributions, these frameworks commonly adopt Feature Pyramid Networks (FPNs) [4] to construct multi-scale feature representations. Consequently, a substantial line of work has focused on strengthening cross-scale feature propagation through FPN variants such as PANet [5], AugFPN [6], and NAS-FPN [7], reflecting the broader trend of improving oriented detection via better multi-scale fusion [8]. Despite these advances, existing pyramid designs typically apply largely uniform fusion strategies across levels, which is often suboptimal in remote sensing scenes where low-level features are vulnerable to background clutter, while high-level semantics must preserve geometry-sensitive cues for oriented localization.

A common direction is to introduce attention or contextual modeling into the pyramid to enhance feature aggregation [9–11]. However, such global modulation often lacks an explicit mechanism to separate foreground from background, especially in scenes containing complex land textures, coastlines, and densely packed instances. Background responses can therefore propagate across pyramid levels, weakening the representation of small or low-contrast objects and amplifying false positives [12]. This suggests that multi-scale fusion should be complemented by targeted, foreground-aware modulation, particularly at lower pyramid levels where spatial details are rich but also most susceptible to clutter.

In parallel, oriented detection crucially depends on modeling object orientation and spatial structure. Prior approaches incorporate orientation cues through proposal-level geometric alignment such as RoI Transformer [13], rotation-equivariant representations as in ReDet [14], and more recent attention- or frequency-driven designs [12, 15, 16]. While effective, these mechanisms are often confined to proposal refinement or a single feature space, and the role of orientation modeling in multi-scale feature interaction remains under-explored. In practice, directional cues can be diluted during cross-level fusion, and background interference further disrupts consistent orientation propagation across scales.

These challenges mirror a broader observation in vision systems: robust performance under complex inputs often benefits from explicitly structured representations and controllable feature modulation rather than relying solely on uniform global mixing. Similar principles have been validated in controllable synthesis and generation, where structured conditioning and selective enhancement of task-relevant regions improve robustness and consistency [17–20]. Motivated by this perspective, we

revisit feature pyramid design for oriented detection and ask how to explicitly inject foreground guidance and orientation-aware interaction into multi-scale fusion.

To this end, we propose a Foreground-Guided Angle-Aware Feature Pyramid Network (FGAA-FPN) built upon Oriented R-CNN for remote sensing oriented object detection. FGAA-FPN explicitly integrates foreground saliency and orientation-aware modeling into the feature pyramid, and adopts a hierarchy-aware design that differentiates processing across pyramid levels. Concretely, we introduce a Foreground-Guided Feature Modulation (FGFM) module to enhance object-related responses in lower-level features and suppress background interference. Meanwhile, we design an Angle-Aware Multi-Head Attention (AAMHA) module at higher pyramid levels to model relative orientation relationships and facilitate geometry-aware global interaction among semantic features. This differentiated design enables more controllable foreground enhancement and more stable orientation information propagation in complex remote sensing scenes.

The main contributions of this paper are summarized as follows:

- We propose Foreground-Guided Feature Modulation (FGFM), which introduces weakly supervised foreground guidance into lower-level pyramid features to enhance object regions and suppress background interference, alleviating foreground–background ambiguity in remote sensing imagery.
- We design Angle-Aware Multi-Head Attention (AAMHA), which explicitly models relative orientation relationships during feature interaction, strengthening the representation of oriented geometric structures in high-level semantic features.
- We construct FGAA-FPN, a novel feature pyramid framework that integrates foreground guidance and angle-aware modeling through differentiated pyramid-level designs, and demonstrate competitive performance on DOTA v1.0 [21] and DOTA v1.5 [21].

2 Related Work

We review oriented object detection in remote sensing imagery, with emphasis on multi-scale feature pyramids, foreground-aware fusion, and orientation-aware modeling, which directly motivate FGAA-FPN.

2.1 Remote Sensing Oriented Object Detection

Remote sensing oriented object detection (RSOD) predicts oriented bounding boxes (OBBS) to better capture object geometry and orientation compared with horizontal boxes [22–24]. Early RSOD frameworks introduce orientation modeling at the detector level. RoI Transformer [13] performs geometric alignment by transforming horizontal proposals into rotated RoIs, while Oriented R-CNN [3] integrates oriented proposals into a two-stage pipeline. More recent efforts focus on handling large scale variation and dense layouts via stronger backbones and receptive field modeling [25–28], for example by using large-kernel contextual encoding [29] or explicit multi-scale perception in the backbone [30]. Despite these advances, how to perform selective

foreground enhancement and orientation-aware propagation during multi-scale fusion remains insufficiently explored in complex remote sensing scenes.

2.2 Multi-scale Pyramids, Foreground-aware Fusion, and Orientation Modeling

Feature Pyramid Networks (FPNs) [4] are widely adopted to address scale variation through multi-level feature fusion. Many general-purpose variants improve information flow or fusion efficiency, including PANet [5], NAS-FPN [7], BiFPN [31], and AugFPN [6]. For remote sensing, several works tailor pyramid designs to enhance small-object cues or robustness under clutter. Representative examples include introducing geometric or foreground perception into pyramids [32], strengthening high-frequency and spatial dependency modeling for small targets [33], and incorporating noise suppression or staged fusion to improve stability in complex backgrounds [1, 34–38]. In parallel, foreground-aware feature learning has been explored by emphasizing target-related regions or saliency cues during fusion, such as region-guided constraints and attention-guided convolution [39, 40], contextual interaction for saliency activation [41, 42], and geometry-aware context modules that couple scale perception with directional cues [43–45].

Another line of work improves oriented localization via explicit geometric modeling. Some approaches enhance shape perception through progressive or multi-branch aggregation [46, 47], while others optimize orientation fitting by dynamic priors or geometry-aware regression losses [48–51]. Overall, existing methods suggest two recurring needs: controllable enhancement of target regions under heavy clutter, and orientation-aware interaction that preserves directional structure beyond the final regression stage. Similar themes appear in controllable generation and editing, where selective modulation and structure-consistent interaction are central to improving fidelity and robustness [52–55]. However, in RSOD, foreground cues are often introduced as static weighting or auxiliary constraints, and orientation modeling is frequently confined to proposal alignment or regression, limiting its impact on multi-scale feature interaction.

In contrast, FGAA-FPN explicitly couples foreground-guided modulation at low pyramid levels with angle-aware multi-head attention at high levels, enabling both target saliency calibration and orientation-aware feature propagation during multi-scale fusion.

3 Proposed Method

In this section, we first present the overall architecture of FGAA-FPN and its integration into the two-stage oriented detector. We then detail the foreground-guided feature modulation (FGFM) for suppressing background noise on low-to-mid pyramid levels, followed by the angle-aware multi-head attention (AAMHA) that injects orientation priors into feature interaction on high-level pyramid features. Finally, we introduce the training objectives, including the box-supervised foreground loss.

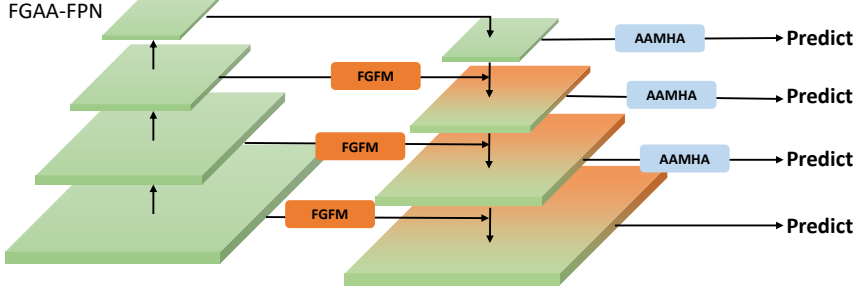


Fig. 1 Overall architecture of the proposed FGAA-FPN. Foreground-guided feature modulation is applied at lower pyramid levels to suppress background interference, while angle-aware feature interaction is introduced at higher levels to enhance orientation modeling. This hierarchical design enables effective integration of foreground discrimination and directional reasoning for oriented object detection.

3.1 Overall framework

FGAA-FPN is built upon a two-stage oriented object detection framework, with Oriented R-CNN adopted as the baseline detector. As shown in Fig. 1, FGAA-FPN serves as an end-to-end feature pyramid network that takes multi-scale backbone features as input and produces hierarchical representations for oriented object detection.

The core design of FGAA-FPN is a hierarchical allocation of functional mechanisms across pyramid levels. Foreground-guided feature modulation(FGFM) module is applied at lower pyramid levels, while Angle-Aware Multi-Head Attention(AAMHA) module is introduced at higher levels. This design is motivated by the distinct characteristics of pyramid features: lower-level features retain fine spatial details and are more vulnerable to background clutter, whereas higher-level features encode stronger semantic context and are better suited for modeling long-range directional relationships.

By enhancing foreground responses and suppressing background interference at lower levels, FGAA-FPN prevents irrelevant information from being amplified during multi-scale feature propagation. At higher levels, angle-aware interaction enables orientation information to directly participate in feature interaction, allowing directional structures to be more consistently preserved across semantic scales. Through this complementary design, FGAA-FPN integrates local foreground discrimination and global orientation modeling within a unified pyramid architecture, leading to more discriminative and structurally coherent feature representations.

3.2 Foreground-Guided Feature Modulation (FGFM)

Foreground-Guided Feature Modulation (FGFM) is designed to enhance foreground representations at early pyramid stages, where features preserve rich spatial details but are highly susceptible to background interference. The overall structure of FGFM is illustrated in Fig. 2. Instead of relying on implicit supervision from downstream detection heads, FGFM explicitly introduces foreground awareness into the feature

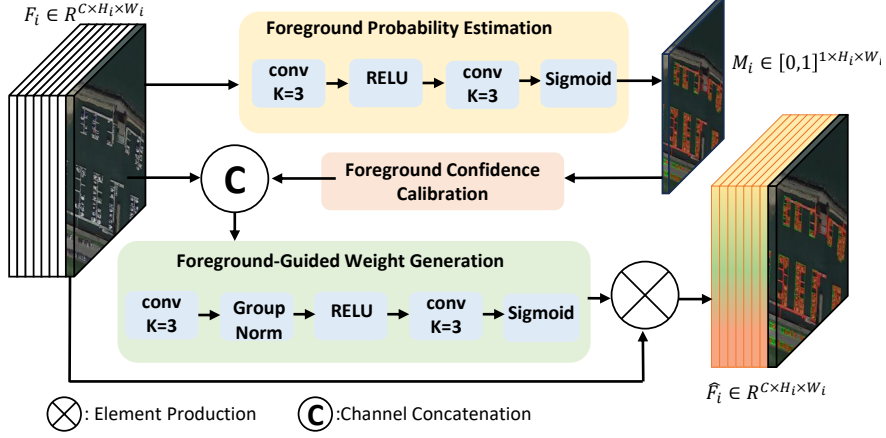


Fig. 2 Overall structure of FGFM. FGFM takes pyramid features as input and first predicts a foreground probability map through a lightweight estimation branch. The predicted foreground confidence is then calibrated and combined with the original features to generate foreground-guided modulation weights. Finally, these weights are applied to reweight the input features, producing foreground-enhanced representations for subsequent detection.

modulation process, enabling more discriminative feature propagation throughout the pyramid.

3.2.1 Foreground Probability Estimation

Foreground-Guided Feature Modulation begins with the explicit estimation of spatial foreground probability at each selected pyramid level. The objective of this step is not to perform precise object segmentation, but to provide a coarse yet reliable foreground prior that distinguishes object-related regions from background clutter in early-stage features.

Let

$$F_i \in \mathbb{R}^{C \times H_i \times W_i} \quad (1)$$

denote the input feature map at the i -th pyramid level, where C is the number of channels and H_i, W_i represent the spatial dimensions.

To preserve spatial resolution while capturing local context, the foreground estimation head is constructed as a lightweight fully convolutional mapping composed of two spatial convolution layers:

$$Z_i = \phi(\mathcal{K}_1(F_i)), \quad (2)$$

$$S_i = \mathcal{K}_2(Z_i), \quad (3)$$

where $\mathcal{K}_1(\cdot)$ and $\mathcal{K}_2(\cdot)$ denote convolutional transformations with spatial kernels, $\phi(\cdot)$ represents a point-wise non-linear activation function, and the intermediate feature Z_i maintains the same spatial resolution as F_i .

The output feature map is then normalized into a probabilistic foreground confidence map via a sigmoid function:

$$M_i = \sigma(S_i), \quad (4)$$

where

$$M_i \in [0, 1]^{1 \times H_i \times W_i} \quad (5)$$

denotes the predicted foreground probability map. Each spatial element $M_i(h, w)$ indicates the likelihood that the location (h, w) belongs to a foreground object.

This design restricts foreground estimation to the spatial domain, avoiding channel-wise competition and ensuring compatibility with multi-scale feature representations. The shallow convolutional structure introduces minimal computational overhead while remaining sensitive to local appearance cues, enabling effective background suppression at lower pyramid levels. Moreover, the foreground probability map M_i is predicted directly from the feature F_i without relying on proposals or detection outputs, allowing FGFM to provide early foreground guidance prior to multi-scale feature propagation.

3.2.2 Calibrated Foreground-Aware Modulation

The foreground probability map M_i provides spatial cues indicating potential object regions. However, directly using M_i for feature modulation may lead to unstable optimization or overly aggressive suppression of ambiguous regions. To address this issue, FGFM introduces a calibrated foreground-aware modulation mechanism that adaptively refines foreground confidence and generates channel-aware modulation weights.

Foreground Confidence Calibration (FCC) is introduced to calibrate the predicted foreground probability map $M_i \in [0, 1]^{1 \times H_i \times W_i}$ by a learnable function, which adjusts the response distribution while preserving training flexibility. The calibrated foreground map is defined as

$$\tilde{M}_i = M_i + \lambda(\sigma(k(M_i - (0.5 + b))) - M_i), \quad (6)$$

where $\sigma(\cdot)$ denotes the sigmoid function, and k , b , and λ are learnable scalar parameters controlling the sharpness, bias, and modulation strength of the calibration process, respectively.

This formulation allows the calibration to degenerate to an identity mapping when $\lambda \rightarrow 0$, ensuring that the original foreground prediction is preserved in early training stages, while enabling progressively sharper foreground separation as optimization proceeds.

Foreground-Guided Weight Generation is designed to generate a channel-wise modulation map based on the calibrated foreground map \tilde{M}_i , conditioning the feature reweighting process on both appearance information and foreground cues. Specifically, the calibrated map is concatenated with the original feature:

$$U_i = \text{Concat}(F_i, \tilde{M}_i), \quad (7)$$

where $U_i \in \mathbb{R}^{(C+1) \times H_i \times W_i}$.

The concatenated feature is then transformed by a lightweight predictor consisting of a spatial convolution, normalization, nonlinearity, and a point-wise projection:

$$T_i = \phi(\text{GN}(\mathcal{K}_3(U_i))), \quad (8)$$

$$M'_i = \sigma(\mathcal{K}_1(T_i)), \quad (9)$$

where $\mathcal{K}_3(\cdot)$ and $\mathcal{K}_1(\cdot)$ denote convolutional transformations with kernel size $K=3$ and $K=1$, respectively, $\text{GN}(\cdot)$ is Group Normalization, $\phi(\cdot)$ is a point-wise activation function, and $\sigma(\cdot)$ is the sigmoid function. The resulting channel-aware modulation map satisfies

$$M'_i \in [0, 1]^{C \times H_i \times W_i}. \quad (10)$$

is the resulting channel-aware modulation map.

3.2.3 Residual Feature Modulation.

The final foreground-modulated feature is obtained via residual scaling:

$$\hat{F}_i = F_i \odot (1 + \alpha M'_i), \quad (11)$$

where \odot denotes element-wise multiplication, α is a learnable or predefined scaling factor, and \hat{F}_i is the output feature after calibrated foreground-aware modulation.

This residual formulation ensures that foreground emphasis acts as a soft and adaptive prior, preserving the original feature structure while selectively enhancing object-related responses. By conditioning modulation on both spatial foreground confidence and channel-wise feature context, FGFM enables stable and effective foreground enhancement at early pyramid levels.

3.3 Angle-Aware Multi-Head Attention (AAMHA)

To preserve directional structures during multi-scale feature refinement, we introduce AAMHA (see Fig. 3), which injects geometry-driven orientation bias and foreground-guided bias into standard multi-head self-attention.

Instead of relying on implicit encoding or deferring orientation reasoning to later regression stages, we explicitly integrate directional awareness into the feature interaction process itself. Multi-head self-attention provides a natural mechanism for modeling long-range spatial dependencies while preserving multiple parallel subspaces, allowing different heads to capture diverse geometric and contextual patterns. Building upon this property, we introduce orientation-aware biases into the attention formulation to guide feature aggregation toward direction-consistent interactions. By conditioning attention weights on relative geometric orientation, the proposed design constrains feature mixing to respect directional structures, alleviating distortion caused by unconstrained global interactions. Furthermore, incorporating foreground-related cues into the attention bias reinforces object-relevant responses and suppresses background interference during feature aggregation. This joint design enables the attention mechanism to simultaneously account for spatial orientation and object

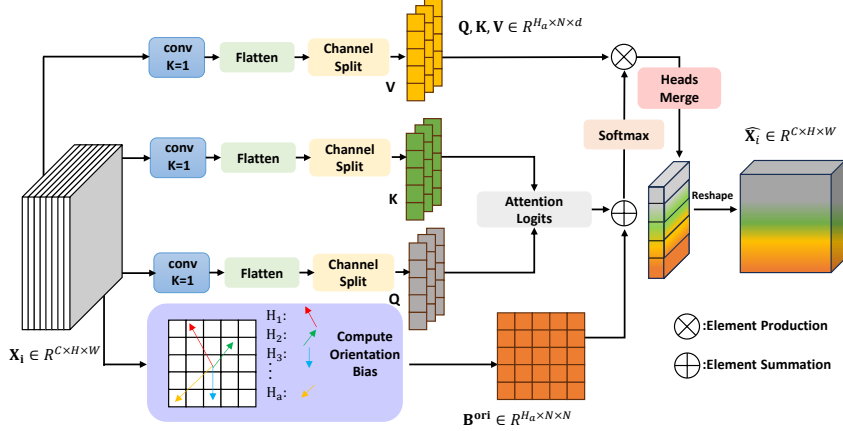


Fig. 3 Overall structure of AAMHA. AAMHA applies multi-head self-attention to pyramid features by projecting them into query, key, and value representations. For each attention head, a learnable orientation prototype is introduced to capture a specific directional preference. Based on normalized relative spatial directions between feature locations, an orientation bias is computed and injected into the attention logits, guiding feature interactions toward direction-consistent responses. The attention outputs from all heads are then aggregated and reshaped back to the original feature space, producing orientation-aware features for subsequent prediction.

saliency, yielding more structured and reliable representations for subsequent oriented object detection.

3.3.1 Multi-head Projection and Tokenization.

Given a pyramid feature map at level i , denoted as $X_i \in \mathbb{R}^{C \times H \times W}$, AAMHA first applies three point-wise projections to obtain query, key and value:

$$Q = \mathcal{P}_q(X_i), \quad K = \mathcal{P}_k(X_i), \quad V = \mathcal{P}_v(X_i), \quad (12)$$

where $\mathcal{P}_q(\cdot)$, $\mathcal{P}_k(\cdot)$, and $\mathcal{P}_v(\cdot)$ are 1×1 convolutions mapping from C to D channels. We split the embedding dimension D into H_a heads with per-head dimension $d = D/H_a$. After flattening the spatial dimension, we obtain

$$Q, K, V \in \mathbb{R}^{H_a \times N \times d}, \quad N = HW, \quad (13)$$

where each spatial location corresponds to one token.

3.3.2 Attention Logits with Orientation Bias.

For standard self-attention, the raw logits for each head are computed as

$$\mathbf{S} = \frac{QK^\top}{\sqrt{d}} \in \mathbb{R}^{H_a \times N \times N}. \quad (14)$$

To model relative directional relationships between any two spatial tokens, we define the 2D coordinate of token p as $\mathbf{c}_p = (x_p, y_p)$. For a token pair (p, q) , the normalized relative direction is

$$\mathbf{u}_{pq} = \frac{\mathbf{c}_p - \mathbf{c}_q}{\|\mathbf{c}_p - \mathbf{c}_q\|_2 + \varepsilon} \in \mathbb{R}^2, \quad (15)$$

where ε is a small constant for numerical stability. Different attention heads are designed to capture distinct directional preferences during feature interaction. To this end, each head h is associated with a learnable orientation vector $\mathbf{w}_h \in \mathbb{R}^2$, which represents the preferred relative direction for that head. The orientation bias for head h is defined as

$$B_h^{\text{ori}}(p, q) = \mathbf{w}_h^\top \mathbf{u}_{pq}. \quad (16)$$

This bias is added to the logits with a scaling factor γ :

$$\mathbf{S} \leftarrow \mathbf{S} + \gamma B^{\text{ori}}. \quad (17)$$

Here $B^{\text{ori}} \in \mathbb{R}^{H_a \times N \times N}$ is constructed by evaluating $B_h^{\text{ori}}(p, q)$ for all heads and token pairs.

3.3.3 Foreground-guided Bias.

Let $M_i \in [0, 1]^{1 \times H \times W}$ denote the foreground probability map produced by FGFM. If its resolution differs from X_i , we bilinearly resize it to (H, W) and flatten it into $\mathbf{m} \in [0, 1]^N$. We then define a foreground-guided bias as

$$B^{\text{fg}}(p, q) = m_p(2m_q - 1), \quad (18)$$

which encourages foreground queries (m_p large) to attend to foreground keys (m_q large) while suppressing attention to background keys (m_q small). This bias is broadcast to all heads and added to logits with a scaling factor β :

$$\mathbf{S} \leftarrow \mathbf{S} + \beta B^{\text{fg}}. \quad (19)$$

3.3.4 Attention Output and Residual Normalization.

The attention weights are computed by softmax over the key dimension:

$$\mathbf{A} = \text{Softmax}(\mathbf{S}), \quad (20)$$

followed by dropout. The output tokens are aggregated as

$$\mathbf{O} = \mathbf{A} \mathbf{V} \in \mathbb{R}^{H_a \times N \times d}, \quad (21)$$

which are then reshaped back to $\mathbb{R}^{D \times H \times W}$ and projected to the original channel dimension by a 1×1 convolution $\mathcal{P}_o(\cdot)$:

$$Y = \mathcal{P}_o(\mathbf{O}). \quad (22)$$

Finally, AAMHA applies residual connection and Group Normalization:

$$\hat{X}_i = \text{GN}(X_i + Y). \quad (23)$$

3.4 Loss Function

To provide explicit foreground priors for feature modulation and attention guidance, FGAA-FPN introduces a foreground branch that predicts spatial foreground probability maps at selected pyramid levels. Given a feature map F_i , the foreground branch outputs a probability map

$$M_i = \mathcal{H}(F_i), \quad M_i \in [0, 1]^{H_i \times W_i}, \quad (24)$$

where $\mathcal{H}(\cdot)$ denotes a shallow convolutional predictor followed by a sigmoid activation. The predicted map encodes the likelihood of each spatial location belonging to a foreground object region and is estimated independently of proposals or detection outputs.

The foreground supervision signal is constructed from ground-truth oriented bounding boxes. For each pyramid level, rotated bounding boxes are projected onto the corresponding feature map resolution, and pixels inside the projected boxes are labeled as foreground, while all remaining locations are treated as background. This process yields a coarse pixel-level ground-truth mask $M_i^{gt} \in \{0, 1\}^{H_i \times W_i}$, which serves as weak supervision without introducing additional annotation cost. If no foreground region exists at a given level for the current mini-batch, the foreground loss at that level is not computed.

Foreground probability maps are supervised using a class-balanced pixel-wise loss that combines weighted binary cross-entropy [56] and Dice loss [57]:

$$\mathcal{L}_{\text{fg}}^{(i)} = \mathcal{L}_{\text{bce}}^{(i)} + \lambda_d \mathcal{L}_{\text{dice}}^{(i)}. \quad (25)$$

The weighted binary cross-entropy term alleviates the severe imbalance between foreground and background pixels, while the Dice loss enforces region-level consistency between the predicted foreground map and the ground-truth mask. The final foreground supervision loss is obtained by averaging $\mathcal{L}_{\text{fg}}^{(i)}$ over all valid pyramid levels and scaling it by a balancing factor λ_{fg} .

To ensure stable optimization and clear functional separation, the predicted foreground probability maps are explicitly detached before being used for feature modulation and attention guidance. As a result, gradients from the detection loss do not propagate into the foreground estimation branch, which is optimized solely through the foreground supervision loss. The overall training objective is defined as

$$\mathcal{L} = \mathcal{L}_{\text{det}} + \lambda_{\text{fg}} \mathcal{L}_{\text{fg}}, \quad (26)$$

where \mathcal{L}_{det} denotes the standard detection loss. This design enables effective foreground learning while preventing the foreground branch from degenerating into an implicit attention mechanism driven by detection objectives.

4 Experiments and discussions

To validate the superiority of the proposed FGAA-FPN, we conduct comprehensive comparisons with multiple state-of-the-art oriented object detection approaches on two large-scale benchmarks, namely DOTAv1.0 and DOTAv1.5.

4.1 Experiment setup

4.1.1 Environmental configuration

All experiments are conducted using the MMRotate framework and implemented in PyTorch. ResNet-50 is adopted as the backbone network for all experiments. During training and inference, input images are resized to a fixed resolution of 1024×1024 . All models are trained on a single NVIDIA RTX 5090 GPU with one image per GPU. The Stochastic Gradient Descent (SGD) optimizer is employed with a momentum of 0.9 and a weight decay of 0.0001. The initial learning rate is set to 0.0025 and is linearly warmed up for the first 500 iterations with a warmup ratio of 1/3, followed by step-wise decay at the 9th and 11th epochs. For DOTA v1.0[21] and DOTA v1.5, models are trained for 12 epochs. Data augmentation includes random resizing and random flipping along horizontal, vertical, and diagonal directions, followed by normalization and padding with a size divisor of 32.

4.1.2 Datasets

DOTA v1.0[21] is a large-scale benchmark for oriented object detection in aerial images, containing 188,282 instances from 15 categories across 2,806 images. The objects exhibit large variations in scale, shape, and orientation, with arbitrary rotations commonly observed in complex scenes. Image resolutions range from approximately 800×800 to $2,000 \times 2,000$ pixels. Following the standard protocol, half of the images are used for training, one-sixth for validation, and the remaining one-third for testing. The annotated categories include Plane (PL), Baseball diamond (BD), Bridge (BR), Ground track field (GTF), Small vehicle (SV), Large vehicle (LV), Ship (SH), Tennis court (TC), Basketball court (BC), Storage tank (ST), Soccer-ball field (SBF), Roundabout (RA), Harbor (HA), Swimming pool (SP), and Helicopter (HC).

DOTA v1.5 extends DOTA v1.0 by introducing an additional category, container crane, and providing extra annotations for small objects with sizes no larger than 10 pixels. This extension significantly increases the total number of instances from 188,282 to 403,318, resulting in denser object distributions and more challenging detection scenarios. The image sources, resolution ranges, and data splitting strategy remain consistent with those of DOTA v1.0.

4.1.3 Evaluation Metrics

To quantitatively evaluate detection performance, we employ AP_{50} , AP_{75} , and mAP as the evaluation metrics in our experiments. The mAP metric measures the mean of average precision values computed under different intersection-over-union (IoU) thresholds, offering a comprehensive indicator of overall detection quality. In contrast, AP_{50} and AP_{75} assess detection accuracy at fixed IoU thresholds of 0.50 and 0.75,

respectively, requiring the predicted bounding boxes to sufficiently overlap with the corresponding ground-truth annotations. Due to the higher overlap requirement, AP_{75} places stronger emphasis on precise object localization and is therefore more sensitive to localization errors than AP_{50} .

4.2 Performance comparison

4.2.1 Comparisons on DOTAv1.0

As shown in Table 1, the proposed **FGAA-FPN** achieves the best overall performance on the DOTA v1.0[21] dataset, reaching an mAP of **75.5%**, and demonstrates strong competitiveness among both one-stage and two-stage detectors. Compared with methods using the same ResNet-50 backbone, such as BVAMFPN and LR-FPN, FGAA-FPN further improves detection accuracy on several challenging categories, including *Ground Track Field*, *Small vehicle*, and *Harbor*, indicating its robustness in complex scenes with diverse object orientations and scales. For instance, FGAA-FPN achieves **77.2%** accuracy on Small vehicle and **65.1%** on Harbor, outperforming existing feature pyramid based approaches.

These improvements can be attributed to the joint design of **foreground-guided feature modulation** and **angle-aware multi-head attention**. By suppressing background interference during early multi-scale feature fusion and explicitly modeling directional information during high-level feature interaction, FGAA-FPN effectively preserves structural and orientation consistency across pyramid levels, leading to more accurate and stable oriented object detection.

4.2.2 Comparisons on DOTAv1.5

As reported in Table 2, all methods are implemented on the same Oriented R-CNN baseline with a ResNet-50 backbone, where only the neck architecture is replaced to ensure a fair comparison. Under this controlled setting, the proposed FGAA-FPN achieves the best overall performance with an mAP of 68.3%, outperforming the strongest competing neck, BVAMFPN (67.4%), by 0.9%.

More importantly, FGAA-FPN demonstrates consistent and pronounced improvements on several orientation-sensitive categories, including Plane, Small Vehicle, Large Vehicle, and particularly Harbor. These object categories are characterized by strong directional structures, elongated shapes, and dense spatial distributions, which place higher demands on orientation modeling and feature alignment. For example, FGAA-FPN raises the detection accuracy for Plane, Small Vehicle, and Large Vehicle to 81.0, 52.5, and 77.1, respectively, and achieves a substantial improvement on Harbor, reaching 75.6, which is significantly higher than that of all other neck designs.

These results indicate that the proposed FGAA-FPN, by strengthening foreground-aware feature propagation and explicitly preserving orientation-consistent representations during multi-scale feature fusion, is particularly effective in suppressing background interference and improving localization accuracy for direction-sensitive objects in cluttered scenes.

Table 1 SOTA comparison on DOTA v1.0.

Methods	Backbone	PL	BD	BR	GTF	SV	LV	SH	TC	BC	ST	SBF	RA	HA	SP	HC	mAP ₅₀
One-stage methods																	
RetinaNet-O ^[58]	ResNet50	88.7	77.6	41.8	58.2	74.6	71.6	79.1	90.3	82.2	74.3	54.8	60.6	62.6	69.7	60.6	68.4
DRN ^[59]	H-104	88.9	80.2	43.5	63.4	73.5	70.7	84.9	90.1	83.9	84.1	50.1	58.4	67.6	68.6	52.5	70.7
PloU ^[60]	DLA-34	80.9	69.7	24.1	60.2	38.3	64.4	64.8	90.9	77.2	70.4	46.5	37.1	57.1	61.9	64.0	60.5
DAL ^[61]	ResNet50	88.7	76.6	45.1	66.8	67.0	76.8	79.7	90.8	79.5	78.5	57.7	62.3	69.1	73.1	60.1	71.4
ClusDet ^[62]	ResNet50	—	—	—	—	—	—	—	—	—	—	—	—	—	—	—	47.6
R3Det ^[63]	ResNet101	88.8	83.1	50.9	67.3	76.2	80.4	86.7	90.8	84.7	84.7	62.0	61.4	66.9	70.6	53.9	73.7
DCL ^[64]	ResNet152	89.1	84.1	50.2	73.6	71.5	58.1	78.0	90.9	86.6	86.8	68.0	67.3	65.6	74.1	67.1	74.1
GWD ^[65]	ResNet101	89.6	81.2	52.9	70.4	77.7	82.4	87.0	89.3	83.1	86.0	64.1	65.1	68.1	71.0	58.5	74.1
AO2-DETR ^[66]	ResNet50	89.3	85.0	56.7	74.9	78.9	82.7	87.4	90.5	84.7	85.4	62.0	70.0	74.7	72.4	71.6	77.7
Two-stage methods																	
Faster R-CNN-O ^[67]	ResNet50	88.4	73.1	44.9	59.1	73.3	71.5	77.1	90.8	78.9	83.9	48.6	63.0	62.2	64.9	56.2	69.1
BoL Transformer ^[13]	ResNet50	88.3	77.1	51.6	69.6	77.5	77.2	87.1	90.8	84.9	83.1	53.0	63.8	74.5	74.5	59.2	73.8
Cascade R-CNN ^[68]	ResNet50	—	—	—	—	—	—	—	—	—	—	—	—	—	—	—	73.5
SCRDet ^[69]	ResNet101	90.0	80.7	52.1	68.4	68.4	60.3	72.4	90.9	87.9	86.9	65.0	66.7	66.3	68.2	65.2	72.6
Gliding vertex ^[70]	ResNet101	89.6	85.0	52.3	77.3	73.0	73.1	86.8	90.7	79.0	86.8	59.6	70.9	72.9	70.9	57.3	75.0
CFA ^[71]	ResNet101	89.3	81.7	51.8	67.2	80.0	78.3	84.5	90.8	83.4	85.5	54.9	67.8	73.0	70.2	65.0	75.1
ARS-DETR ^[72]	ResNet50	87.0	75.6	48.3	69.2	77.9	77.9	87.7	90.5	77.3	82.9	60.3	64.6	74.9	71.8	66.6	74.2
MutDet ^[73]	ResNet50	87.3	78.7	51.3	68.5	78.9	81.6	88.1	90.7	79.9	83.7	58.0	61.8	76.5	72.1	60.8	74.5
GCL ^[74]	ResNet50	89.1	83.2	43.3	76.4	79.1	77.5	83.1	90.1	84.1	85.1	64.2	65.5	66.2	75.4	58.7	74.7
LR-FPN ^[75]	ResNet50	89.5	74.5	42.5	64.9	77.9	75.5	84.0	91.0	81.3	83.7	56.6	63.5	65.4	60.9	36.3	69.7
SFANet ^[76]	ResNet50	89.1	83.1	50.8	77.0	77.8	74.2	86.3	90.9	86.6	85.3	60.9	63.5	64.3	68.3	54.1	74.2
BVAMFPN ^[77]	ResNet50	89.2	83.5	46.4	75.8	76.7	72.3	84.5	89.4	85.4	86.8	67.6	64.4	71.6	65.9	75.2	75.5
FGAA-FPN(Ours)	ResNet50	89.4	83.9	46.9	76.3	77.2	72.5	84.7	89.2	85.5	87.2	68.3	67.8	65.1	71.8	66.7	75.5

Table 2 SOTA comparison on DOTA v1.5.

Neck	PL	BD	BR	GTF	SV	LV	SH	TC	BC	ST	SBF	RA	HA	SP	HC	CC	mAP ₅₀
NAS_FPN[7]	79.9	78.3	54.4	68.8	52.2	76.2	87.2	90.8	78.5	68.2	55.8	80.6	67.3	66.1	48.2	12.3	66.6
PAFPN[5]	79.5	81.4	52.2	71.0	52.2	76.3	80.9	90.9	81.2	68.5	59.9	72.3	67.4	64.3	56.8	17.3	67.0
PaFPN[78]	79.4	79.5	53.2	70.9	51.9	76.5	80.9	90.9	81.4	68.4	55.9	71.3	64.8	51.8	47	65.6	
CE_FPN[79]	79.0	79.9	53.2	70.9	51.6	76.5	80.9	90.8	80.4	67.6	60.8	70.3	66.6	68.1	59.6	6.1	66.1
BAFPN[80]	80.1	83.0	54.4	71.6	52.4	76.5	87.1	90.9	79.2	68.9	62.7	73.2	68.1	65.0	56.9	17.3	68.1
BVAMFPN[77]	80.1	81.2	49.4	70.5	51.2	76.8	87.1	90.7	78.2	68.9	62.7	72.9	72.1	65.2	59.6	12.1	67.4
FGAA-FPN(Ours)	81.0	81.2	53.1	72.2	52.5	77.1	87.2	90.6	78.9	69.1	63.3	72.2	75.6	65.9	60.3	12.5	68.3

4.3 Ablation Studies and Analysis

The previous section has demonstrated the superiority of the proposed FGAA-FPN over a range of state-of-the-art methods. We further conduct ablation studies to uncover the intrinsic factors behind its performance gains. Unless otherwise specified, all experiments are performed on DOTA v1.5 using Oriented R-CNN with a ResNet-50 backbone under identical settings, where only the neck configurations are modified for fair comparison. In the tables, P3–P7 denote the feature pyramid levels, with P3 being the highest-resolution (fine-grained) feature map and P7 the lowest-resolution (high-level) feature map, typically formed by successive $2\times$ downsampling across levels.

4.3.1 Role of individual modules

Table 3 Component ablation of FGAA-FPN on DOTA v1.5 under the same Oriented R-CNN (R-50) baseline.

Method	FGFM Lv.	AAMHA Lv.	mAP ₅₀	mAP ₇₅
Baseline (FPN)	–	–	64.4	41.7
+ FGFM only	P3–P5	–	67.1	43.6
+ AAMHA only	–	P5–P7	66.3	43.1
FGAA-FPN (Full)	P3–P5	P5–P7	<u>68.3</u>	<u>44.1</u>

As shown in Table 3, enabling each component individually yields clear improvements over the baseline. With **FGFM** deployed on pyramid levels **P3–P5**, the detector achieves a **2.7%** increase in mAP₅₀ and a **1.9%** increase in mAP₇₅, confirming the effectiveness of foreground-guided modulation on high-resolution features. When **AAMHA** is applied alone on **P5–P7**, an orientation bias with $\gamma = 0.7$ is used at all these levels, resulting in a **1.9%** increase in mAP₅₀ and a **1.4%** increase in mAP₇₅, which validates the benefit of angle-aware attention for orientation-consistent feature interaction at higher semantic levels.

Furthermore, combining **FGFM** on **P3–P5** with **AAMHA** on **P5–P7** leads to the most pronounced improvements, achieving a **3.9%** increase in mAP₅₀ and a **2.4%** increase in mAP₇₅. In this full setting, the mask bias is additionally enabled only at **P5** with $\beta = 0.6$ to strengthen foreground-to-foreground interactions on the boundary level where the two modules meet. These results suggest that the two components are complementary: **FGFM** enhances fine-grained foreground cues, while **AAMHA** strengthens direction-aware contextual aggregation, and their synergy yields the best overall performance.

4.3.2 Influence of Level Placement and Cost-Effectiveness.

Before analyzing the placement results in Table 4, we clarify the meaning of the reported complexity metrics. **Parameters** refer to the number of learnable weights,

Table 4 Ablation on level placement. Only one module is enabled in each block; all other settings remain identical.

Setting	FGFM Lv.	AAMHA Lv.	mAP ₅₀	Parameters	FLOPs
(A) FGFM placement (AAMHA disabled)					
FGFM@low	P3–P5	–	67.1	3.79M	72.20G
FGFM@high	P5–P7	–	65.2	<u>3.78M</u>	<u>60.25G</u>
FGFM@all	P3–P7	–	66.2	4.08M	72.39G
(B) AAMHA placement (FGFM disabled)					
AAMHA@low	–	P3–P5	66.2	4.12M	77.21G
AAMHA@high	–	P5–P7	66.3	<u>3.61M</u>	<u>60.88G</u>
AAMHA@all	–	P3–P7	66.5	4.37M	80.94G

and **FLOPs** denote the floating-point operations required for a forward pass. Importantly, both metrics are computed **only for the neck** (i.e., FGAA-FPN and its variants), rather than the entire Oriented R-CNN detector, so that the cost variation is solely attributed to different neck designs.

FGFM placement. As shown in Block (A) of Table IV, placing FGFM on **P3–P5** achieves the best performance, reaching **67.1** mAP₅₀, while moving FGFM to higher levels (**P5–P7**) causes a clear drop to **65.2**. This behavior is consistent with the design goal of FGFM: it relies on foreground probability estimation to modulate features, and such estimation is more reliable at higher-resolution levels where spatial details and object boundaries are preserved. In contrast, at high pyramid levels the feature maps have much lower resolution, and small or thin objects are more likely to be blurred into surrounding background. As a result, the foreground mask becomes less accurate and the modulation can be misled by false positives/false negatives, which ultimately degrades detection quality. Applying FGFM to all levels (**P3–P7**) does not further improve the result (**66.2**), indicating that extending modulation to coarse levels introduces limited benefit while increasing complexity, since it still inherits the risk of unreliable foreground estimation on low-resolution maps.

AAMHA placement. Block (B) of Table IV evaluates AAMHA placement with FGFM disabled and $\beta = 0$ to isolate the effect of orientation-aware attention. Although applying AAMHA to all levels (**P3–P7**) yields the highest mAP₅₀ (**66.5**), this gain is marginal compared with applying it only to high levels (**P5–P7, 66.3**) or low levels (**P3–P5, 66.2**). In contrast, the computational overhead varies substantially with the placement. Specifically, restricting AAMHA to **P5–P7** incurs the lowest cost with only **3.61M** parameters and **60.88G** FLOPs, whereas applying AAMHA to all levels increases the overhead to **4.37M** parameters and **80.94G** FLOPs. This indicates that the performance differences across placements are small, yet the complexity gap is large, making the all-level deployment *cost-inefficient*. Moreover, the design of AAMHA naturally favors high-level placement: attention-based interaction is particularly meaningful when features are semantically stable and less dominated by local noise, and higher pyramid levels provide a more suitable abstraction for modeling long-range orientation-consistent relationships. Therefore, considering both accuracy and efficiency, deploying AAMHA on **P5–P7** is a more cost-effective choice.

4.3.3 Impact of AAMHA Bias Terms

Table 5 Ablation of AAMHA bias terms under the FGAA-FPN setting.

Method	γ	β	mAP ₅₀	mAP ₇₅
AAMHA (w/o bias)	0.0	0.0	66.2	43.2
AAMHA + Orient	0.7	0.0	68.0	44.1
AAMHA + Mask	0.0	0.6	67.2	43.5
AAMHA (Full)	0.7	0.6	<u>68.3</u>	<u>44.1</u>

As shown in Table 5, different bias designs in AAMHA lead to distinct performance gains under the FGAA-FPN setting, where FGFM is fixed on P3–P5 as described in the main text. Here, **w/o bias** disables both bias terms ($\gamma=0, \beta=0$), **+ Orient** enables only the orientation bias ($\gamma=0.7, \beta=0$), and **+ Mask** enables only the mask bias ($\gamma=0, \beta=0.6$).

Compared with **w/o bias**, introducing the orientation bias yields the most pronounced improvement, achieving a **1.8%** increase in mAP₅₀ and a **0.9%** increase in mAP₇₅. In contrast, enabling only the mask bias results in more modest gains of **1.0%** on mAP₅₀ and **0.3%** on mAP₇₅, indicating that foreground-guided modulation alone is less effective than explicitly modeling directional relationships. When both bias terms are jointly applied, **AAMHA (Full)** attains the best overall performance on both metrics, achieving **68.3%** on mAP₅₀ and **44.1%** on mAP₇₅ demonstrating that the mask bias provides complementary benefits to the orientation bias.

This behavior is consistent with the design of AAMHA. The orientation bias explicitly injects relative directional cues into attention logits, which promotes orientation-consistent feature interaction and is particularly beneficial for stricter localization accuracy as reflected by mAP₇₅. In contrast, the mask bias mainly regularizes attention to focus on foreground regions, enhancing object-centric aggregation without directly encoding geometric direction, and thus yields limited standalone improvement. Their combination therefore leads to more robust and balanced performance.

4.3.4 Generalization across Detectors

To verify the plug-and-play applicability of FGAA-FPN beyond a single architecture, we further replace the original FPN with FGAA-FPN in several representative oriented detectors and report the results in Fig. 4. FGAA-FPN consistently improves performance across all baselines, including Rotated Faster R-CNN, RoITransformer, Gliding Vertex, Rotated RetinaNet, and Oriented R-CNN. Notably, the gains are stable and non-trivial, with improvements of **1.5%**, **0.3%**, **1.2%**, **0.7%**, and **2.8%** mAP, respectively. These results indicate that the proposed design is not tailored to a specific detector head, but instead provides a generally effective feature fusion backbone by jointly enhancing foreground-aware propagation and orientation-consistent interaction, thereby validating the effectiveness of our FGAA-FPN design.

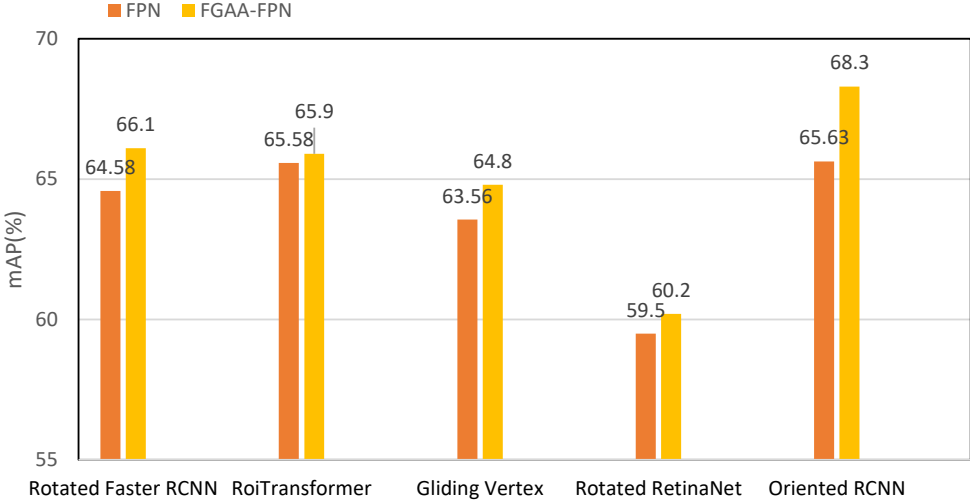


Fig. 4 Generalization across detectors on DOTA v1.5. We replace the original FPN with FGAA-FPN in several representative oriented detectors under identical settings. FGAA-FPN consistently improves mAP, demonstrating its plug-and-play applicability.

4.4 Visualization

Visualization results on the DOTA v1.5 dataset are presented in Fig. 5, where three rows correspond to the detection outputs of the baseline Oriented R-CNN, the proposed FGAA-FPN, and the ground truth, respectively. Compared with the baseline, our method produces more accurate oriented bounding boxes with better alignment to object geometry, especially for densely distributed and arbitrarily oriented targets.

In addition, FGAA-FPN effectively reduces both false positives and missed detections in complex scenes, leading to more complete and consistent object coverage. These improvements can be attributed to the complementary effects of the proposed modules. FGFM enhances foreground-aware feature propagation, allowing the model to focus on object regions across scales, while AAMHA explicitly strengthens orientation-consistent feature interaction, resulting in more reliable geometric representation. Benefiting from these designs, FGAA-FPN achieves more precise and robust detection performance in challenging remote sensing scenarios.

5 Conclusion

In this work, we propose FGAA-FPN, a foreground-guided and angle-aware feature pyramid network for oriented object detection in remote sensing imagery. FGAA-FPN enhances multi-scale feature fusion by introducing foreground-guided feature modulation to strengthen target responses in lower-level features and angle-aware multi-head attention to promote orientation-consistent interaction among higher-level semantic features. Experiments on DOTA v1.0 and DOTA v1.5 show that FGAA-FPN consistently improves detection performance over strong baselines, while ablation studies

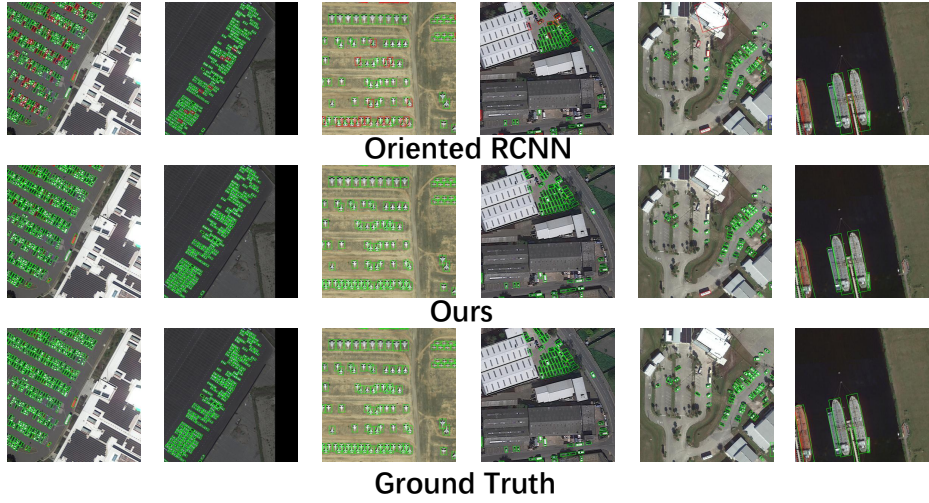


Fig. 5 Visualizations of detection results on DOTAv1.5. Failures are marked by red boxes

confirm that the two modules provide complementary benefits. Although effective, FGAA-FPN introduces additional computational cost, and its foreground guidance is learned under weak supervision from bounding-box annotations, which may be sub-optimal in highly cluttered scenes or settings with noisy labels. Future work will focus on more lightweight designs and more informative geometric and semantic priors to further improve efficiency and generalization across diverse remote sensing detection scenarios.

References

- [1] Zhang, X., Zhang, T., Wang, G., Zhu, P., Tang, X., Jia, X., Jiao, L.: Remote sensing object detection meets deep learning: A metareview of challenges and advances. *IEEE Geoscience and Remote Sensing Magazine* **11**(4), 8–44 (2023)
- [2] Khelifi, L., Mignotte, M.: Deep learning for change detection in remote sensing images: Comprehensive review and meta-analysis. *Ieee Access* **8**, 126385–126400 (2020)
- [3] Xie, X., Cheng, G., Wang, J., Yao, X., Han, J.: Oriented r-cnn for object detection. In: *Proceedings of the IEEE/CVF International Conference on Computer Vision*, pp. 3520–3529 (2021)
- [4] Lin, T.-Y., Dollár, P., Girshick, R., He, K., Hariharan, B., Belongie, S.: Feature pyramid networks for object detection. In: *Proceedings of the IEEE Conference on Computer Vision and Pattern Recognition*, pp. 2117–2125 (2017)
- [5] Liu, S., Qi, L., Qin, H., Shi, J., Jia, J.: Path aggregation network for instance

segmentation. In: Proceedings of the IEEE Conference on Computer Vision and Pattern Recognition, pp. 8759–8768 (2018)

[6] Guo, C., Fan, B., Zhang, Q., Xiang, S., Pan, C.: Augfpn: Improving multi-scale feature learning for object detection. In: Proceedings of the IEEE/CVF Conference on Computer Vision and Pattern Recognition, pp. 12595–12604 (2020)

[7] Ghiasi, G., Lin, T.-Y., Le, Q.V.: Nas-fpn: Learning scalable feature pyramid architecture for object detection. In: Proceedings of the IEEE/CVF Conference on Computer Vision and Pattern Recognition, pp. 7036–7045 (2019)

[8] Gong, Y., Yu, X., Ding, Y., Peng, X., Zhao, J., Han, Z.: Effective fusion factor in fpn for tiny object detection. In: Proceedings of the IEEE/CVF Winter Conference on Applications of Computer Vision, pp. 1160–1168 (2021)

[9] Du, Z., Liang, Y.: Object detection of remote sensing image based on multi-scale feature fusion and attention mechanism. *IEEE Access* **12**, 8619–8632 (2024)

[10] Wang, G., Gan, X., Cao, Q., Zhai, Q.: Mfanet: multi-scale feature fusion network with attention mechanism. *The Visual Computer* **39**(7), 2969–2980 (2023)

[11] Han, H., Zhang, Q., Li, F., Du, Y.: Foreground capture feature pyramid network-oriented object detection in complex backgrounds. *IEEE Transactions on Neural Networks and Learning Systems* **36**(4), 6925–6939 (2024)

[12] Min, K., Lee, G.-H., Lee, S.-W.: Attentional feature pyramid network for small object detection. *Neural Networks* **155**, 439–450 (2022)

[13] Ding, J., Xue, N., Long, Y., Xia, G.-S., Lu, Q.: Learning roi transformer for oriented object detection in aerial images. In: Proceedings of the IEEE/CVF Conference on Computer Vision and Pattern Recognition, pp. 2849–2858 (2019)

[14] Han, J., Ding, J., Xue, N., Xia, G.-S.: Redet: A rotation-equivariant detector for aerial object detection. In: Proceedings of the IEEE/CVF Conference on Computer Vision and Pattern Recognition, pp. 2786–2795 (2021)

[15] Qin, Z., Zhang, P., Wu, F., Li, X.: Fcanet: Frequency channel attention networks. In: Proceedings of the IEEE/CVF International Conference on Computer Vision, pp. 783–792 (2021)

[16] Fu, R., Chen, C., Yan, S., Zhang, R., Wang, X., Chen, H.: Fadl-net: Frequency-assisted dynamic learning network for oriented object detection in remote sensing images. *IEEE Transactions on Industrial Informatics* **20**(8), 9939–9951 (2024)

[17] Shen, F., Tang, J.: Imagpose: A unified conditional framework for pose-guided

person generation. *Advances in neural information processing systems* **37**, 6246–6266 (2024)

[18] Shen, F., Ye, H., Zhang, J., Wang, C., Han, X., Wei, Y.: Advancing pose-guided image synthesis with progressive conditional diffusion models. In: The Twelfth International Conference on Learning Representations (2024). <https://openreview.net/forum?id=rHzapPnCgT>

[19] Shen, F., Ye, H., Liu, S., Zhang, J., Wang, C., Han, X., Wei, Y.: Boosting consistency in story visualization with rich-contextual conditional diffusion models. In: Proceedings of the AAAI Conference on Artificial Intelligence, vol. 39, pp. 6785–6794 (2025)

[20] Shen, F., Jiang, X., He, X., Ye, H., Wang, C., Du, X., Li, Z., Tang, J.: Imagdressing-v1: Customizable virtual dressing. In: Proceedings of the AAAI Conference on Artificial Intelligence, vol. 39, pp. 6795–6804 (2025)

[21] Xia, G.-S., Bai, X., Ding, J., Zhu, Z., Belongie, S., Luo, J., Datcu, M., Pelillo, M., Zhang, L.: Dota: A large-scale dataset for object detection in aerial images. In: Proceedings of the IEEE Conference on Computer Vision and Pattern Recognition, pp. 3974–3983 (2018)

[22] Nie, G., Huang, H.: Multi-oriented object detection in aerial images with double horizontal rectangles. *IEEE Transactions on Pattern Analysis and Machine Intelligence* **45**(4), 4932–4944 (2022)

[23] Xu, C., Ding, J., Wang, J., Yang, W., Yu, H., Yu, L., Xia, G.-S.: Dynamic coarse-to-fine learning for oriented tiny object detection. In: Proceedings of the IEEE/CVF Conference on Computer Vision and Pattern Recognition, pp. 7318–7328 (2023)

[24] Cánovas-García, F., Alonso-Sarría, F., Gomariz-Castillo, F., Oñate-Valdivieso, F.: Modification of the random forest algorithm to avoid statistical dependence problems when classifying remote sensing imagery. *Computers & Geosciences* **103**, 1–11 (2017)

[25] Deng, Z., Sun, H., Zhou, S., Zhao, J., Lei, L., Zou, H.: Multi-scale object detection in remote sensing imagery with convolutional neural networks. *ISPRS journal of photogrammetry and remote sensing* **145**, 3–22 (2018)

[26] Zhang, Y., Yuan, Y., Feng, Y., Lu, X.: Hierarchical and robust convolutional neural network for very high-resolution remote sensing object detection. *IEEE Transactions on Geoscience and Remote Sensing* **57**(8), 5535–5548 (2019)

[27] Wang, G., Zhuang, Y., Chen, H., Liu, X., Zhang, T., Li, L., Dong, S., Sang, Q.: Fsod-net: Full-scale object detection from optical remote sensing imagery. *IEEE Transactions on Geoscience and Remote Sensing* **60**, 1–18 (2021)

- [28] Dong, Z., Wang, M., Wang, Y., Zhu, Y., Zhang, Z.: Object detection in high resolution remote sensing imagery based on convolutional neural networks with suitable object scale features. *IEEE Transactions on Geoscience and Remote Sensing* **58**(3), 2104–2114 (2019)
- [29] Li, Y., Li, X., Dai, Y., Hou, Q., Liu, L., Liu, Y., Cheng, M.-M., Yang, J.: Lsknet: A foundation lightweight backbone for remote sensing: Y. li et al. *International Journal of Computer Vision* **133**(3), 1410–1431 (2025)
- [30] Cai, X., Lai, Q., Wang, Y., Wang, W., Sun, Z., Yao, Y.: Poly kernel inception network for remote sensing detection. In: *Proceedings of the IEEE/CVF Conference on Computer Vision and Pattern Recognition*, pp. 27706–27716 (2024)
- [31] Chen, J., Mai, H., Luo, L., Chen, X., Wu, K.: Effective feature fusion network in bifpn for small object detection. In: *2021 IEEE International Conference on Image Processing (ICIP)*, pp. 699–703 (2021). IEEE
- [32] Ren, D., Liu, Y., Sun, H., Zhang, L., Wan, J.: Hierarchical heterogeneous geometric foreground perception network for remote sensing object detection. *IEEE Transactions on Geoscience and Remote Sensing* (2025)
- [33] Shi, Z., Hu, J., Ren, J., Ye, H., Yuan, X., Ouyang, Y., He, J., Ji, B., Guo, J.: Hs-fpn: High frequency and spatial perception fpn for tiny object detection. In: *Proceedings of the AAAI Conference on Artificial Intelligence*, vol. 39, pp. 6896–6904 (2025)
- [34] Chang, Y., Yan, L., Wu, T., Zhong, S.: Remote sensing image stripe noise removal: From image decomposition perspective. *IEEE Transactions on Geoscience and Remote Sensing* **54**(12), 7018–7031 (2016)
- [35] Niu, R., Zhi, X., Jiang, S., Gong, J., Zhang, W., Yu, L.: Aircraft target detection in low signal-to-noise ratio visible remote sensing images. *Remote Sensing* **15**(8), 1971 (2023)
- [36] Ma, X., Dong, J., Wei, W., Zheng, B., Ma, J., Zhou, T.: Remote sensing image object detection by fusing multi-scale contextual features and channel enhancement. In: *2023 International Joint Conference on Neural Networks (IJCNN)*, pp. 01–07 (2023). IEEE
- [37] Zhang, K., Shen, H.: Multi-stage feature enhancement pyramid network for detecting objects in optical remote sensing images. *Remote Sensing* **14**(3), 579 (2022)
- [38] Jiang, H., Qian, Y., Yang, G., Liu, H.: Mlknet: Multi-stage for remote sensing image spatiotemporal fusion network based on a large kernel attention. *IEEE Journal of Selected Topics in Applied Earth Observations and Remote Sensing* **17**, 1257–1268 (2023)

- [39] Wang, Z., Tian, H., Yang, W., Xu, Z., Chen, W., Li, Y., Xu, T., Liu, J., Wang, Z.: Foreground attention loss and attention-guided convolution for remote sensing object detection. *IEEE Sensors Journal* (2025)
- [40] Xu, Z.-l., Tang, W., Wu, P.-f.: Aerial object detection in complex scenes based on mask guidance. In: 2023 3rd International Conference on Computer Science, Electronic Information Engineering and Intelligent Control Technology (CEI), pp. 505–510 (2023). IEEE
- [41] Xu, Y., Ji, H.: Contextual-semantic interactive perception network for small object detection in uav aerial images. *Remote Sensing* **17**(21), 3581 (2025)
- [42] Lu, W., Chen, S.-B., Ding, C.H., Tang, J., Luo, B.: Lwganet: A lightweight group attention backbone for remote sensing visual tasks. *arXiv preprint arXiv:2501.10040* (2025)
- [43] Yang, D., Wu, F., Qu, G., Liu, Y., Cheng, Y., Aramayo, A., Zheng, Z., Yang, Z.: Lgm-det: A lightweight geometry-aware multi-scale detector for oriented ship target detection in sar images. *IEEE Journal of Selected Topics in Applied Earth Observations and Remote Sensing* (2025)
- [44] Chen, Y., Wang, Z., Xiong, Z., Zhang, Y., Xu, X.: Soam block: A scale-orientation-aware module for efficient object detection in remote sensing imagery. *Symmetry* **17**(8), 1251 (2025)
- [45] Hu, Z., Meng, X., Liu, X., Sun, Z.: Rotation-invariant feature enhancement with dual-aspect loss for arbitrary-oriented object detection in remote sensing. *Applied Sciences* **15**(10), 5240 (2025)
- [46] Zhu, Y., Lv, K., Yu, Y., Xu, W.: Edge-guided parallel network for vhr remote sensing image change detection. *IEEE Journal of Selected Topics in Applied Earth Observations and Remote Sensing* **16**, 7791–7803 (2023)
- [47] Wu, Y., Zhang, K., Wang, J., Wang, Y., Wang, Q., Li, X.: Gcwnet: A global context-weaving network for object detection in remote sensing images. *IEEE Transactions on Geoscience and Remote Sensing* **60**, 1–12 (2022)
- [48] Min, L., Gao, K., Wang, H., Wang, J., Yu, P., Li, T., Chen, Z.: Remote sensing image scene classification using deep combinative feature learning. In: AOPC 2020: Optical Sensing and Imaging Technology, vol. 11567, pp. 646–652 (2020). SPIE
- [49] Qian, W., Yang, X., Peng, S., Zhang, X., Yan, J.: Rsdet++: Point-based modulated loss for more accurate rotated object detection. *IEEE Transactions on Circuits and Systems for Video Technology* **32**(11), 7869–7879 (2022)
- [50] Gan, L., Tan, X., Hu, L.: Gws: Rotation object detection in aerial remote sensing

images based on gauss–wasserstein scattering. *AI Communications* **37**(1), 169–183 (2024)

- [51] Zhou, Z., Zhu, Y.: Kldet: Detecting tiny objects in remote sensing images via kullback–leibler divergence. *IEEE transactions on geoscience and remote sensing* **62**, 1–16 (2024)
- [52] Shen, F., Xu, W., Yan, R., Zhang, D., Shu, X., Tang, J.: Imagedit: Let any subject transform. *arXiv preprint arXiv:2510.01186* (2025)
- [53] Shen, F., Du, X., Gao, Y., Yu, J., Cao, Y., Lei, X., Tang, J.: Imagharmony: Controllable image editing with consistent object quantity and layout. *arXiv preprint arXiv:2506.01949* (2025)
- [54] Shen, F., Yu, J., Wang, C., Jiang, X., Du, X., Tang, J.: Imaggarment-1: Fine-grained garment generation for controllable fashion design. *arXiv preprint arXiv:2504.13176* (2025)
- [55] Shen, F., Wang, C., Gao, J., Guo, Q., Dang, J., Tang, J., Chua, T.-S.: Long-term talkingface generation via motion-prior conditional diffusion model. In: *Forty-second International Conference on Machine Learning*
- [56] Ruby, U., Yendapalli, V., et al.: Binary cross entropy with deep learning technique for image classification. *Int. J. Adv. Trends Comput. Sci. Eng* **9**(10) (2020)
- [57] Li, X., Sun, X., Meng, Y., Liang, J., Wu, F., Li, J.: Dice loss for data-imbalanced nlp tasks. In: *Proceedings of the 58th Annual Meeting of the Association for Computational Linguistics*, pp. 465–476 (2020)
- [58] Lin, T.-Y., Goyal, P., Girshick, R., He, K., Dollár, P.: Focal loss for dense object detection. In: *Proceedings of the IEEE International Conference on Computer Vision*, pp. 2980–2988 (2017)
- [59] Zheng, G., Zhang, F., Zheng, Z., Xiang, Y., Yuan, N.J., Xie, X., Li, Z.: Drn: A deep reinforcement learning framework for news recommendation. In: *Proceedings of the 2018 World Wide Web Conference*, pp. 167–176 (2018)
- [60] Chen, Z., Chen, K., Lin, W., See, J., Yu, H., Ke, Y., Yang, C.: Piou loss: Towards accurate oriented object detection in complex environments. In: *European Conference on Computer Vision*, pp. 195–211 (2020). Springer
- [61] Ming, Q., Zhou, Z., Miao, L., Zhang, H., Li, L.: Dynamic anchor learning for arbitrary-oriented object detection. In: *Proceedings of the AAAI Conference on Artificial Intelligence*, vol. 35, pp. 2355–2363 (2021)
- [62] Yang, F., Fan, H., Chu, P., Blasch, E., Ling, H.: Clustered object detection in aerial images. In: *Proceedings of the IEEE/CVF International Conference on*

Computer Vision, pp. 8311–8320 (2019)

[63] Yang, X., Yan, J., Feng, Z., He, T.: R3det: Refined single-stage detector with feature refinement for rotating object. In: Proceedings of the AAAI Conference on Artificial Intelligence, vol. 35, pp. 3163–3171 (2021)

[64] Yang, X., Hou, L., Zhou, Y., Wang, W., Yan, J.: Dense label encoding for boundary discontinuity free rotation detection. In: Proceedings of the IEEE/CVF Conference on Computer Vision and Pattern Recognition, pp. 15819–15829 (2021)

[65] Yang, X., Yan, J., Ming, Q., Wang, W., Zhang, X., Tian, Q.: Rethinking rotated object detection with gaussian wasserstein distance loss. In: International Conference on Machine Learning, pp. 11830–11841 (2021). PMLR

[66] Dai, L., Liu, H., Tang, H., Wu, Z., Song, P.: Ao2-detr: Arbitrary-oriented object detection transformer. IEEE Transactions on Circuits and Systems for Video Technology **33**(5), 2342–2356 (2022)

[67] Ren, S., He, K., Girshick, R., Sun, J.: Faster r-cnn: Towards real-time object detection with region proposal networks. IEEE transactions on pattern analysis and machine intelligence **39**(6), 1137–1149 (2016)

[68] Cai, Z., Vasconcelos, N.: Cascade r-cnn: Delving into high quality object detection. In: Proceedings of the IEEE Conference on Computer Vision and Pattern Recognition, pp. 6154–6162 (2018)

[69] Yang, X., Yang, J., Yan, J., Zhang, Y., Zhang, T., Guo, Z., Sun, X., Fu, K.: Scrdet: Towards more robust detection for small, cluttered and rotated objects. In: Proceedings of the IEEE/CVF International Conference on Computer Vision, pp. 8232–8241 (2019)

[70] Xu, Y., Fu, M., Wang, Q., Wang, Y., Chen, K., Xia, G.-S., Bai, X.: Gliding vertex on the horizontal bounding box for multi-oriented object detection. IEEE transactions on pattern analysis and machine intelligence **43**(4), 1452–1459 (2020)

[71] Guo, Z., Liu, C., Zhang, X., Jiao, J., Ji, X., Ye, Q.: Beyond bounding-box: Convex-hull feature adaptation for oriented and densely packed object detection. In: Proceedings of the IEEE/CVF Conference on Computer Vision and Pattern Recognition, pp. 8792–8801 (2021)

[72] Zeng, Y., Chen, Y., Yang, X., Li, Q., Yan, J.: Ars-detr: Aspect ratio-sensitive detection transformer for aerial oriented object detection. IEEE transactions on geoscience and remote sensing **62**, 1–15 (2024)

[73] Huang, Z., Feng, Y., Liu, Q., Wang, Y.: Mutdet: Mutually optimizing pre-training

for remote sensing object detection. In: European Conference on Computer Vision, pp. 1–17 (2024). Springer

[74] Ming, Q., Miao, L., Zhou, Z., Song, J., Pizurica, A.: Gradient calibration loss for fast and accurate oriented bounding box regression. *IEEE transactions on geoscience and remote sensing* **62**, 1–15 (2024)

[75] Li, H., Zhang, R., Pan, Y., Ren, J., Shen, F.: Lr-fpn: Enhancing remote sensing object detection with location refined feature pyramid network. In: 2024 International Joint Conference on Neural Networks (IJCNN), pp. 1–8 (2024). IEEE

[76] Liu, H., Ma, S., Xia, D., Li, S.: Sfanet: A spectrum-aware feature augmentation network for visible-infrared person reidentification. *IEEE Transactions on Neural Networks and Learning Systems* **34**(4), 1958–1971 (2021)

[77] Wang, Z., Yang, J., Qiao, Y., Zhang, W.: Bvamfpn: multi-scale feature fusion for rotated object detection in remote sensing based on biological visual attention mechanism. *Journal of Real-Time Image Processing* **23**(1), 26 (2026)

[78] Huang, S., Lu, Z., Cheng, R., He, C.: Fapn: Feature-aligned pyramid network for dense image prediction. In: Proceedings of the IEEE/CVF International Conference on Computer Vision, pp. 864–873 (2021)

[79] Luo, Y., Cao, X., Zhang, J., Guo, J., Shen, H., Wang, T., Feng, Q.: Ce-fpn: enhancing channel information for object detection. *Multimedia Tools and Applications* **81**(21), 30685–30704 (2022)

[80] Li, J., Wang, Q., Dong, H.: Bafpn: bidirectionally aligning features to improve object localization accuracy in remote sensing images. *Applied Intelligence* **55**(16), 1071 (2025)